

RESEARCH ARTICLE | SEPTEMBER 09 2022

Nanostructured back surface amorphization of silicon with picosecond laser pulses

Markus Blothe ; Maxime Chambonneau ; Stefan Nolte



Appl. Phys. Lett. 121, 101602 (2022)

<https://doi.org/10.1063/5.0103276>



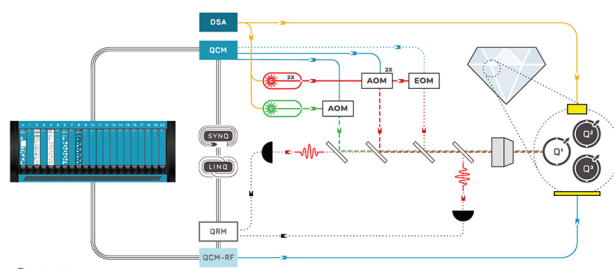
CrossMark



QBLOX

Integrates all
Instrumentation + Software
for Control and Readout of

Superconducting Qubits
NV-Centers
Spin Qubits



Nanostructured back surface amorphization of silicon with picosecond laser pulses

Cite as: Appl. Phys. Lett. **121**, 101602 (2022); doi: [10.1063/5.0103276](https://doi.org/10.1063/5.0103276)

Submitted: 15 June 2022 · Accepted: 17 August 2022 ·

Published Online: 9 September 2022



View Online



Export Citation



CrossMark

Markus Blothe,^{1,a)}  Maxime Chambonneau,¹  and Stefan Nolte^{1,2} 

AFFILIATIONS

¹Friedrich Schiller University Jena, Institute of Applied Physics, Abbe Center of Photonics, Albert-Einstein-Straße 15, Jena 07745, Germany

²Fraunhofer Institute for Applied Optics and Precision Engineering IOF, Center of Excellence in Photonics, Albert-Einstein-Straße 7, Jena 07745, Germany

^{a)}Author to whom correspondence should be addressed: markus.blothe@uni-jena.de

ABSTRACT

Laser-based amorphization on the back surface of a 525- μm thick crystalline silicon sample is studied. To deposit sufficient energy for a local change from a crystalline to an amorphous state, laser irradiation at 2- μm wavelength with 25-ps pulse duration is combined with Bessel beam shaping. Deterministic single-site modifications and homogeneous continuous lines of amorphous silicon are demonstrated. Optical and electron microscopy together with Raman spectroscopy measurements highlight the material transformations featuring the formation of subwavelength periodic surface structures. The investigations open up possibilities for processing in-built microelectronic devices.

© 2022 Author(s). All article content, except where otherwise noted, is licensed under a Creative Commons Attribution (CC BY) license (<http://creativecommons.org/licenses/by/4.0/>). <https://doi.org/10.1063/5.0103276>

Silicon is the backbone material of the semiconductor and electronics industry. A wide range of its properties including electrical conductivity and optical reflectivity strongly depend on the state of the material—especially when one compares the crystalline (c-Si) and the amorphous (a-Si) state. Despite lower electronic performance than c-Si, a-Si is commonly used for different applications (e.g., in solar cells and thin-film transistors).^{1,2} The standard techniques to produce a-Si are chemical vapor deposition, sputtering, and ion bombardment.^{3,4} However, those methods suffer from important drawbacks such as the need for a hot environment during deposition and permanently induced impurities. A promising alternative method for inducing a state transformation due to its fast and contactless nature relies on laser irradiation. A prominent example for laser-based silicon processing is laser crystallization, where an a-Si layer is transformed into a polycrystalline state.⁵ Conversely, the production of an a-Si layer by picosecond laser radiation was already investigated more than 40 years ago,⁶ and the later development of ultrafast lasers allowed different groups to demonstrate surface amorphization of c-Si with various irradiation parameters.^{7–12} So far, this laser-based amorphization technique is solely applied to the front surface of silicon. The possibility to amorphize the back surface is highly desirable for manufacturing, processing, and modifying the properties of in-built microelectronic devices. Moreover, back surface processing usually shows numerous

advantages, as it is cleaner because the re-deposition of debris is minimized, no plasma shielding effects hinder energy deposition,^{13–15} and the energy deposition can be more efficient due to an evolving absorption front in the material which moves toward the laser.^{16,17} However, filamentation makes it challenging to produce permanent modifications both in the bulk and on the back surface of monolithic silicon.¹⁸ This originates from (i) the intensity clamping phenomenon which saturates the energy deposition in the material, and (ii) the nonlinear focal shift causing an out-of-focus interaction zone.^{19–24} Taken together, these two nonlinear mechanisms lead to a strongly delocalized energy deposition in silicon when femtosecond laser pulses are employed. This delocalization process is further enhanced in the case of tightly focused diffractive beams by the refractive index mismatch at the air–silicon interface which causes severe spherical aberration.^{18,24–26}

In this Letter, a method based on picosecond laser irradiation with a Bessel beam shape for amorphizing the back surface of c-Si is investigated. Single-site laser-produced modifications consisting of ring-shaped a-Si features are observed. Interestingly, laser-induced periodic surface structures (LIPSS), which scatter visible light, are detected, thus making the produced a-Si layer appearing black when observed with optical bright-field microscopy in reflection. We demonstrate the inscription of continuous lines consisting of a

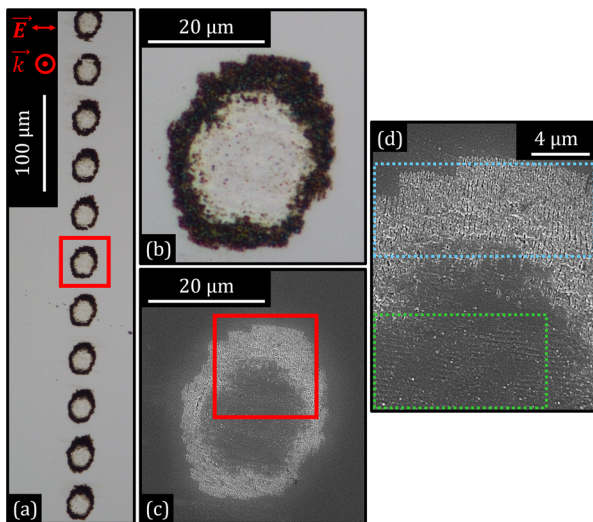


FIG. 1. (a) Optical bright-field micrograph in reflection of modifications produced at the back surface after irradiation with 1250 pulses with $4.1 \mu\text{J}$ pulse energy. \vec{E} and \vec{k} indicate the polarization and the writing beam propagation direction, respectively. (b) Magnification of the red rectangle area in (a). (c) SEM image of the exact same modification as in (b). (d) Magnification of the red rectangle area in (c). The blue and green rectangles indicate regions of subwavelength structures perpendicular and parallel to the polarization, respectively.

homogeneous layer of a-Si on the back surface. Similar to the front surface configuration, a maskless wet etching process can be envisioned,²⁷ and surface waveguides can be realized.^{4,11} The produced LIPSS on the back surface also hold promises due to the changes in the absorption and reflection of light, wettability, and tribological properties.²⁸

A double-side polished, $525\text{-}\mu\text{m}$ thick silicon wafer with $\langle 100 \rangle$ surface orientation and a resistivity $>200 \Omega \text{ cm}$ is used in the experiments. It is positioned with sub-micrometer precision by means of a three-axis stage system relative to the focal position. The back surface of the sample is irradiated with pulses delivered by a customized thulium-doped fiber laser (Active Fiber Systems GmbH)²⁹ operating at $1.96\text{-}\mu\text{m}$ center wavelength ensuring increased energy deposition in the infrared spectral region.²⁰ The transform-limited pulses of 275 fs are stretched to 25 ps (full-width at half-maximum) by fine-tuning the compressor of the laser in order to decrease nonlinear propagation effects by lowering the peak intensity and still avoid a large heat-affected zone.³⁰ The repetition rate is chosen as low as 12.5 kHz to avoid heat accumulation on a pulse-to-pulse basis.^{9,24} The pulse energy measured after the focusing optics is adjusted by the combination of a half-wave plate and a polarizer. The final polarization state of the beam is controlled by an additional half-wave plate placed before the focusing optics. An axicon is used to transform the Gaussian beam profile (2 mm diameter at $1/e^2$) into a Bessel beam, in order to benefit from diffraction-free propagation and suppress spherical aberration caused by the refractive index mismatch at the air–silicon interface. The focal region is demagnified with a factor of 34 toward the back surface of the sample by a two-lens setup in the 4-f configuration consisting of a spherical lens ($f = 200 \text{ mm}$) and an aspheric lens ($f = 5.9 \text{ mm}$).

The experimental arrangement is described in detail in the [supplementary material](#), Fig. S1. An analogous arrangement for producing micro-Bessel beams is described in Ref. 31. Linear calculations predict an interference region length (depth of focus, DOF) of 57 and $219 \mu\text{m}$ in air and silicon, respectively, with a central maximum diameter of $2.35 \mu\text{m}$ at $1/e^2$. *Ex-situ* surface characterizations are carried out with optical bright-field microscopy in reflection, scanning electron microscopy (SEM), and confocal Raman spectroscopy (numerical aperture $\text{NA} = 0.85$). The employed wavelength for Raman spectroscopy (532 nm) is chosen to provide a high resolution and to selectively probe a very limited depth because of the high absorption coefficient ($>10^4 \text{ cm}^{-1}$) of silicon at this wavelength.

Let us first examine the outcome of single-site irradiations on the back surface with pulse energies ranging from 1.4 up to $9.7 \mu\text{J}$ with 1250 pulses. An exemplary optical micrograph of 11 modifications under identical conditions (1250 pulses, $4.1 \mu\text{J}$ pulse energy) is displayed in Fig. 1(a). These modifications consist of a drastically reduced reflective zone in a hollow ring-like shape. Other number of applied pulses (313 and 125 000) have been tested, all leading to comparable observations. Similar appearance from one site to another demonstrates the deterministic character of the process. The overall size of the modification scales with the employed pulse energy within the tested range. In contrast to the femtosecond Bessel beam configuration which does not allow attaining the regime of permanent modification on the back surface of silicon,³¹ it is important to highlight that the employed picosecond Bessel beam enables us to modify the material in a deterministic way. This notable difference likely originates from the reduced nonlinear effects and the increased thermal effects when the pulse duration is increased. A magnification of the modification indicated in red in Fig. 1(a) is shown in Fig. 1(b), where a continuous black ellipse with small variations in width is observed. The corresponding minor and major axes are 24.5 and $32 \mu\text{m}$, respectively. One may note the one order-of-magnitude difference between these dimensions and the linearly calculated central maximum diameter of the beam ($2.35 \mu\text{m}$). This might be explained by nonlinear propagation effects, which strongly affect the fluence distribution on the back surface, as experimentally observed elsewhere³¹—therefore can lead to the detected increase in size. The contribution of the second ($2.6 \mu\text{m}$ apart from the central maximum with $I/I_0 = 0.16$) and subsequent maxima of the Bessel beam and heat diffusion^{32,33} should play only a minor role for the increase in size. One can note that the minor axis is oriented along the direction of the linear polarization. Non-symmetric modifications were also observed by other groups in the bulk for multi-pulse irradiation,^{18,30} but the orientation toward the polarization is turned by 90° at the back surface. Additionally, a slight change in reflection for the central zone in comparison to the surrounding pristine material can be observed. The same modification is visible with SEM in Fig. 1(c). These observations together with further analysis of the cross section of a modified site (see Fig. S2 in the [supplementary material](#)) allow us to conclude that there is no major material ablation at the micrometer scale. The striking feature of the comparison between optical and electron microscopy micrographs shown in Figs. 1(b) and 1(c) is the inverted intensity contrast of the ellipse which appears darker and brighter than the surrounding, respectively. This is partly explained by the SEM magnification in Fig. 1(d), which reveals a major topographical change on the nanometer scale in the form of LIPSS with two different alignments, along and perpendicular to the

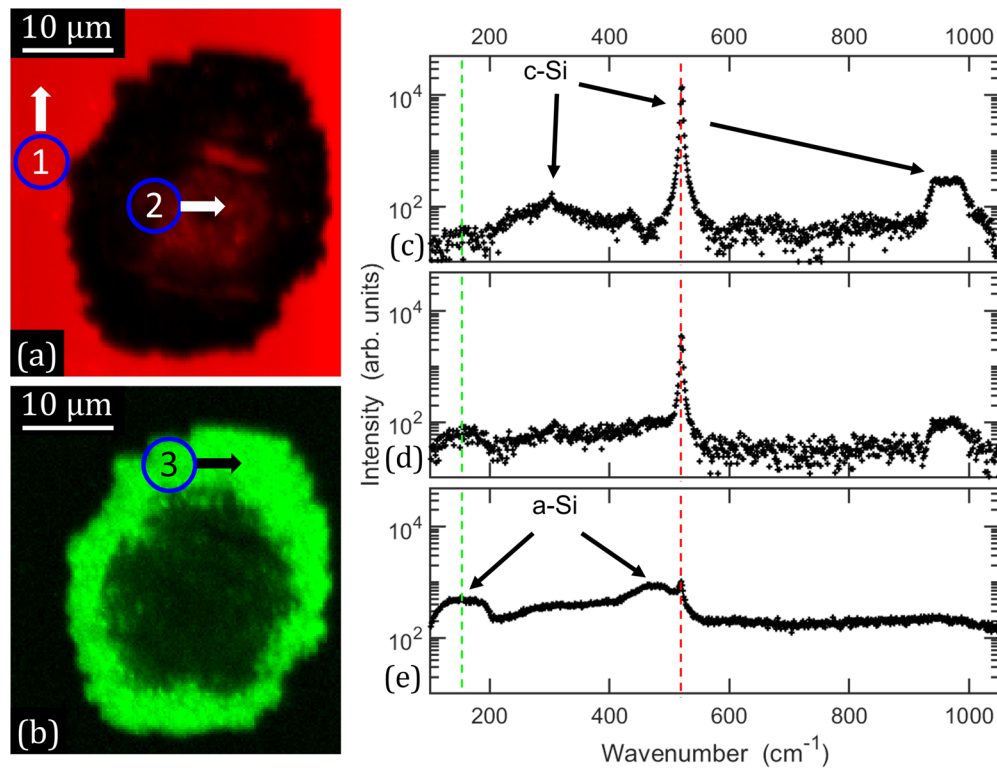


FIG. 2. Normalized amplitude distribution of the Raman signal at (a) 520 and (b) 150 cm^{-1} , attributed to c-Si and a-Si, respectively. (c)–(e) Raman spectra corresponding to the marked positions (1)–(3) in (a) and (b). The vertical dashed lines indicate the wavenumbers used in (a) and (b).

polarization, in the green and blue rectangles, respectively. The LIPSS period is estimated to be 320 ± 52 nm for the inner and 310 ± 55 nm for the outer regions. The presence of nano-structures, which scatter visible light, provides an explanation to the dark appearance of the ellipses in Figs. 1(a) and 1(b). The bright appearance of these ellipses under SEM [Figs. 1(c) and 1(d)] could originate from a local modification of the electrical properties of silicon. One can assume that c-Si has been locally amorphized, as the electrical conduction of a-Si can be orders of magnitude lower than that of undoped c-Si.^{34,35}

To examine the hypothesis of a change from c-Si to a-Si at the back surface, confocal Raman spectroscopy has been carried out on the same site as in Figs. 1(b)–1(d). Results of these Raman spectroscopy measurements are represented in Figs. 2(a) and 2(b) by color maps corresponding to the amplitude of the signal at 520 cm^{-1} (red) and 150 cm^{-1} (green). These two wavenumbers have been selected as 520 cm^{-1} is the single-phonon peak of c-Si³⁶ and 150 cm^{-1} corresponds to one of the wavenumber regions (100–200 cm^{-1}), which is inherent to a-Si signal with no overlap with any c-Si signal.³⁷ The comparison between the two color maps allows us to conclude that the modification in Figs. 1(b) and 1(c) corresponds to an amorphous region. The heavily altered region matches almost perfectly with the a-Si signal. This is confirmed in Figs. 2(c)–2(e) where Raman spectra at different measurement points indicated in Figs. 2(a) and 2(b) are displayed. These spectra plotted in semi-logarithmic scale correspond to

(1) a pristine region, (2) the central part of the modification, and (3) the outer ring structure. By comparing the measured spectra on points (1) and (2) [Figs. 2(c) and 2(d)], one may note a decrease in the amplitude of the main c-Si peak at 520 cm^{-1} in the center part with respect to pristine silicon. This can be explained by the formation of defects in the crystal lattice induced by the laser irradiation. The slight appearance of a-Si features in Fig. 2(d) suggests a coexistence of crystalline and amorphous states. In contrast, barely no c-Si main peak signal is observed in the ring-shaped region, and the a-Si features dominate the acquired spectrum in Fig. 2(e). One can, thus, conclude that in this region, the silicon is almost completely amorphized. One may note the apparent contradiction between the measured amorphization in Fig. 2 and the decreased reflectivity in optical microscopy [see Figs. 1(a) and 1(b)]. Indeed, as the refractive index of a-Si is higher than that of c-Si, one would expect an increased reflectivity in the amorphized areas. The decreased reflectivity in Figs. 1(a) and 1(b) originates from the observed LIPSS in Fig. 1(d) which scatter visible light.

One should mention that similar a-Si ring formation was observed in the case of Gaussian femtosecond pulses focused on the front surface of c-Si.^{7,10,12} Various models have been developed for identifying the underlying physical mechanisms, including thermal^{6,7,10–12} and non-thermal^{27,38} melting, as well as resolidification processes at different cooling rates. In these models, the center part shows a lower cooling rate, giving the atoms sufficient time to re-form

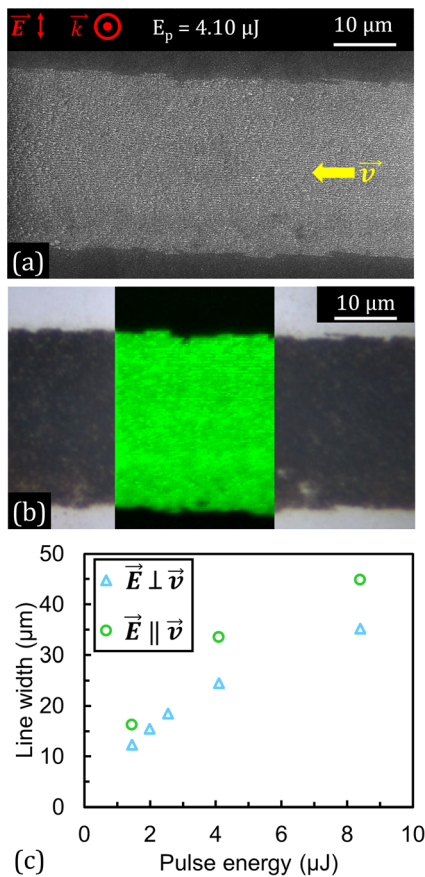


FIG. 3. (a) SEM image of a typical line produced by moving the c-Si sample at a speed of $50 \mu\text{m s}^{-1}$ during irradiation (pulse energy $4.1 \mu\text{J}$). \vec{E} , \vec{v} , and \vec{k} indicate the polarization, the writing direction, and the propagation direction of the writing beam, respectively. (b) Optical bright-field micrograph in reflection of the same line as in (a) with superimposed Raman spectroscopy measurements at 150 cm^{-1} similar to Fig. 2(b). (c) Evolution of the linewidth as a function of the pulse energy for different polarizations. The standard deviation for 20 measurements at different positions of a line reached a maximum value of $\approx 2.5 \mu\text{m}$.

a crystalline lattice while the outer regions freeze in an amorphous state. Such a physical explanation could also be applied in our picosecond back surface irradiation configuration. However, an additional degree of complexity for the modeling lies in the nonlinear propagation effects, which govern the energy deposition in silicon.

While we concentrated so far on the production of modifications on the back surface with single-site irradiations, let us now explore the resulting morphology when the sample is moved continuously at a speed of $50 \mu\text{m s}^{-1}$ during irradiation. An SEM image of a typical resulting continuous line is displayed in Fig. 3(a). As discussed above, the fact that the line appears brighter than the unmodified silicon suggests that it solely corresponds to a-Si with an increased surface roughness. The formation of a homogeneous a-Si layer is confirmed by the Raman spectroscopy measurements superimposed on an optical micrograph in Fig. 3(b). Similar to Fig. 2(b), the green color corresponds to an a-Si feature measured at 150 cm^{-1} . The Raman spectrum

corresponding to Fig. 3(b) (not shown here) is similar to the one in Fig. 2(e). We, thus, conclude that moving the sample during the irradiation results in the production of a homogeneous line of a-Si on the back surface.

The evolution of the linewidth as a function of the pulse energy has also been investigated. The results obtained with a polarization parallel and perpendicular to the writing direction are shown in Fig. 3(c). For both polarization states, the linewidth increases with the pulse energy. This suggests that the energy deposition at the exit surface of silicon is not saturated by nonlinear propagation effects in the tested configuration (25-ps pulses of $1.4\text{--}8.4\text{-}\mu\text{J}$ energy). One may note that, for identical pulse energy, wider lines are observed when the polarization is parallel to the writing direction. This is in agreement with the above-discussed elliptical shape for single-site modifications, whose major axis is perpendicular to the polarization (see Fig. 1). The ratio between the major and minor axes of single-site modifications (≈ 1.3) corresponds in Fig. 3(c) to the ratio between the linewidths written with parallel and perpendicular polarization with respect to the writing direction. Therefore, the linewidth can be controlled by adjusting the pulse energy as well as the input polarization.

Ultimately, one can distinguish in Fig. 3(a) single-orientation LIPSS in the laser-written a-Si line. Given the strong dependence of LIPSS on the polarization,³⁹ let us now examine the LIPSS orientation and period in our experimental conditions. High-magnification SEM images of the laser-written lines are displayed in Figs. 4(a) and 4(b) for a polarization perpendicular and parallel to the writing direction, respectively. The trenches and ridges are systematically perpendicular to the polarization, meaning that the LIPSS orientation can be tuned by rotating the electric field. Nanometer-sized grain-like structures are randomly distributed over the imaged areas and might resemble redeposited nano-particles. To determine the LIPSS period, 100 sites have been analyzed for each image. The corresponding histograms are shown in Figs. 4(c) and 4(d), for a polarization perpendicular and parallel to the writing direction, respectively. The observed periods are in the $200\text{--}400 \text{ nm}$ range, with average values of 306 and 276 nm for the LIPSS shown in Figs. 4(a) and 4(b), respectively. These values are in excellent agreement with a typical LIPSS period given by the formula $\lambda/2n = 284 \text{ nm}$,³⁹ where $n = 3.45$ is the refractive index of silicon at the laser wavelength $\lambda = 1.96 \mu\text{m}$.

To summarize, we have demonstrated that deterministic modifications can be produced on the back surface of c-Si with picosecond Bessel beams at $2 \mu\text{m}$ wavelength. Single-site modifications consist of ring-shaped a-Si layers exhibiting subwavelength structures. By continuously moving the sample during irradiation, homogeneous a-Si lines have been produced, and their width can be controlled by adjusting the pulse energy and the polarization. These lines exhibit LIPSS perpendicular to the polarization, with a period around $\lambda/2n$. While the increased index of a-Si with respect to c-Si would normally make the lines appear bright under optical microscopy, the presence of LIPSS scattering visible light makes these appear dark. Overall, this laser-based method offers an additional degree of freedom for selectively amorphizing c-Si on the back surface, which could be used in integrated silicon electronics industry. The presented technique can potentially be transferred to other bandgap materials as well as long as it is transparent to the laser radiation. In the future, further studies including single-pulse irradiation, pulse-to-pulse evolution, and front surface irradiation will be carried out.

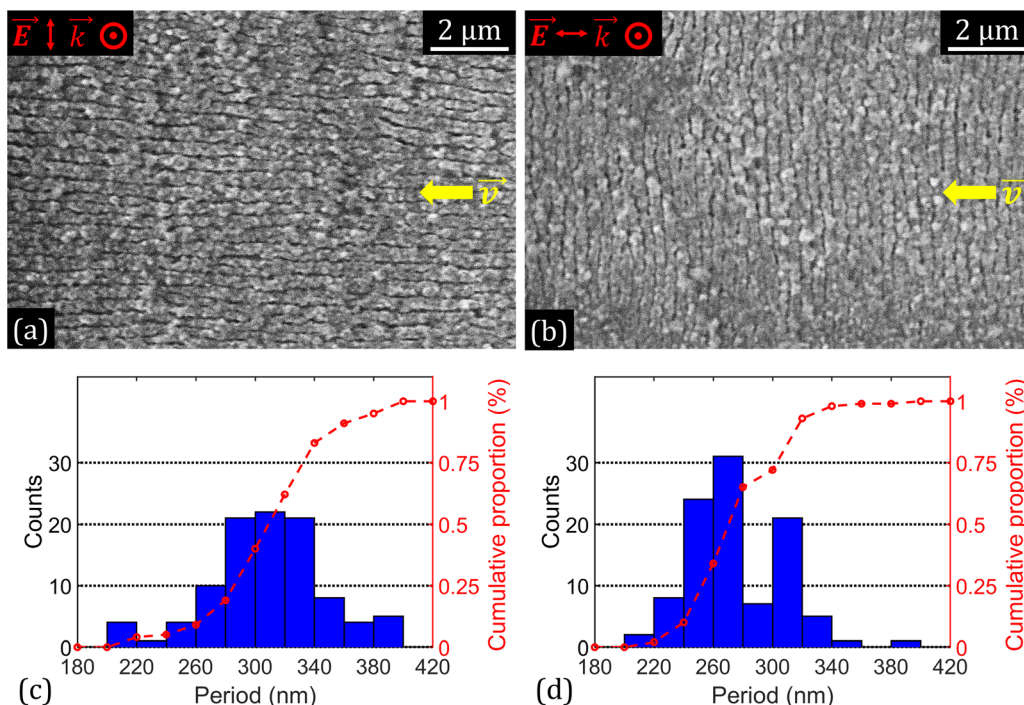


FIG. 4. SEM images of lines written with polarization \vec{E} (a) perpendicular and (b) parallel to the writing direction \vec{v} . (c) and (d) Histograms of the period distribution in 20 nm wide categories for the structures shown in (a) and (b), respectively.

See the [supplementary material](#) for a schematic of the inscription setup and a cross-sectional observation of an amorphized track.

The authors highly appreciate the work of Christiane Otto for sample preparation. The authors are grateful to Qingfeng Li for linear Bessel beam calculation code and to Tobias Heuermann for technical support for laser operation. M.B. thanks TRUMPF GmbH + Co. KG for financial support.

AUTHOR DECLARATIONS

Conflict of Interest

The authors have no conflicts to disclose.

Author Contributions

Markus Blothe: Conceptualization (lead); Investigation (lead); Visualization (lead); Writing – original draft (lead); Writing – review & editing (lead). **Maxime Chambonneau:** Conceptualization (equal); Visualization (supporting); Writing – original draft (supporting); Writing – review & editing (equal). **Stefan Nolte:** Funding acquisition (lead); Project administration (lead); Resources (lead); Supervision (lead); Writing – review & editing (equal).

DATA AVAILABILITY

The data that support the findings of this study are available from the corresponding author upon reasonable request.

REFERENCES

- ¹T. Sameshima, M. Hara, and S. Usui, *Jpn. J. Appl. Phys.* **28**, 1789 (1989).
- ²S. D. Wolf, A. Descocudres, Z. C. Holman, and C. Ballif, *Green* **2**, 7 (2012).
- ³A. R. Forouhi and I. Bloomer, *Phys. Rev. B* **34**, 7018 (1986).
- ⁴M. J. De Dood, A. Polman, T. Zijlstra, and E. W. Van Der Drift, *J. Appl. Phys.* **92**, 649 (2002).
- ⁵J. S. Im, H. J. Kim, and M. O. Thompson, *Appl. Phys. Lett.* **63**, 1969 (1993).
- ⁶P. L. Liu, R. Yen, N. Bloembergen, and R. T. Hodgson, *Appl. Phys. Lett.* **34**, 864 (1979).
- ⁷J. Bonse, K.-W. Brzezinka, and A. Meixner, *Appl. Surf. Sci.* **221**, 215 (2004).
- ⁸M. Garcia-Lechuga, D. Puerto, Y. Fuentes-Edfuf, J. Solis, and J. Siegel, *ACS Photonics* **3**, 1961 (2016).
- ⁹I. Gnilitzkiy, V. Gruzdev, N. M. Bulgakova, T. Mocek, and L. Orazi, *Appl. Phys. Lett.* **109**, 143101 (2016).
- ¹⁰Y. Fuentes-Edfuf, M. Garcia-Lechuga, D. Puerto, C. Florian, A. Garcia-Leis, S. Sanchez-Cortes, J. Solis, and J. Siegel, *Appl. Phys. Lett.* **110**, 211602 (2017).
- ¹¹M. Garcia-Lechuga, N. Casquero, A. Wang, D. Grojo, and J. Siegel, *Adv. Opt. Mater.* **9**, 2100400 (2021).
- ¹²C. Florian, D. Fischer, K. Freiberg, M. Duwe, M. Sahre, S. Schneider, A. Hertwig, J. Krüger, M. Rettenmayr, U. Beck, A. Undisz, and J. Bonse, *Mater.* **14**, 1651 (2021).
- ¹³N. L. Boling, M. D. Crisp, and G. Dubé, *Appl. Opt.* **12**, 650 (1973).
- ¹⁴S. Papernov and A. W. Schmid, *J. Appl. Phys.* **104**, 063101 (2008).
- ¹⁵E. Allahyari, J. JJ Nivas, M. Valadan, R. Fittipaldi, A. Vecchione, L. Parlato, R. Bruzzese, C. Altucci, and S. Amoroso, *Appl. Surf. Sci.* **488**, 128 (2019).
- ¹⁶E. Ohmura, F. Fukuyo, K. Fukumitsu, and H. Morita, *J. Achiev. Mater. Manuf. Eng.* **17**, 381 (2006); available at http://jamme.acmssse.h2.pl/papers_amme06/193.pdf.
- ¹⁷C. W. Carr, J. D. Bude, and P. DeMange, *Phys. Rev. B* **82**, 184304 (2010).
- ¹⁸M. Chambonneau, D. Grojo, O. Tokel, F. O. Ilday, S. Tzortzakis, and S. Nolte, *Laser Photonics Rev.* **15**, 2100140 (2021).

- ¹⁹V. V. Kononenko, E. V. Zavedeev, and V. M. Gololobov, *Appl. Phys. A* **122**, 293 (2016).
- ²⁰E. V. Zavedeev, V. V. Kononenko, and V. I. Konov, *Laser Phys.* **26**, 016101 (2016).
- ²¹M. Chanal, V. Y. Fedorov, M. Chambonneau, R. Clady, S. Tzortzakis, and D. Grojo, *Nat. Commun.* **8**, 773 (2017).
- ²²M. Chambonneau, Q. Li, V. Y. Fedorov, M. Blothe, K. Schaarschmidt, M. Lorenz, S. Tzortzakis, and S. Nolte, *Laser Photonics Rev.* **15**, 2000433 (2021).
- ²³E. I. Mareev, K. V. Lvov, B. V. Rumiantsev, E. A. Migal, I. D. Novikov, S. Y. Stremoukhov, and F. V. Potemkin, *Laser Phys. Lett.* **17**, 015402 (2020).
- ²⁴M. Chambonneau, M. Blothe, Q. Li, V. Y. Fedorov, T. Heuermann, M. Gebhardt, C. Gaida, S. Tertelmann, F. Sotier, J. Limpert, S. Tzortzakis, and S. Nolte, *Phys. Rev. Res.* **3**, 043037 (2021).
- ²⁵Q. Li, M. Chambonneau, M. Blothe, H. Gross, and S. Nolte, *Appl. Opt.* **60**, 3954 (2021).
- ²⁶A. Wang, A. Das, J. Hermann, and D. Grojo, *Appl. Phys. Lett.* **119**, 041108 (2021).
- ²⁷A. Kiani, K. Venkatakrishnan, and B. Tan, *Opt. Express* **17**, 16518 (2009).
- ²⁸J. Bonse and S. Gräf, *Nanomaterials* **11**, 3326 (2021).
- ²⁹M. Baudisch, M. Beutler, M. Gebhardt, C. Gaida, F. Stutzki, S. Hadrich, R. Herda, K. Zawilski, P. Schunemann, A. Zach, J. Limpert, and I. Rimke, *Laser Congress (ASSL)* (2018), Vol. 3.
- ³⁰A. Das, A. Wang, O. Uteza, and D. Grojo, *Opt. Express* **28**, 26623 (2020).
- ³¹D. Grojo, A. Mouskeftaras, P. Delaporte, and S. Lei, *J. Appl. Phys.* **117**, 153105 (2015).
- ³²V. V. Kononenko, E. V. Zavedeev, M. I. Latushko, and V. I. Konov, *Laser Phys. Lett.* **10**, 036003 (2013).
- ³³J. Bonse, T. Seuthe, M. Grehn, M. Eberstein, A. Rosenfeld, and A. Mermillod-Blondin, *Appl. Phys. A* **124**, 60 (2018).
- ³⁴W. Fulkerson, J. P. Moore, R. K. Williams, R. S. Graves, and D. L. McElroy, *Phys. Rev.* **167**, 765 (1968).
- ³⁵W. Beyer and B. Hoheisel, *Solid State Commun.* **47**, 573 (1983).
- ³⁶J. H. Parker, D. W. Feldman, and M. Ashkin, *Phys. Rev.* **155**, 712 (1967).
- ³⁷D. Beeman, R. Tsu, and M. F. Thorpe, *Phys. Rev. B* **32**, 874 (1985).
- ³⁸V. P. Lipp, B. Rethfeld, M. E. Garcia, and D. S. Ivanov, *Phys. Rev. B* **90**, 245306 (2014).
- ³⁹J. Bonse and S. Gräf, *Laser Photonics Rev.* **14**, 2000215 (2020).